

Anomalous decay and scattering processes of the η meson

Bastian Kubis^{1,2}, Judith Plenter¹

¹Helmholtz-Institut für Strahlen- und Kernphysik, Universität Bonn, D-53115 Bonn, Germany

²Bethe Center for Theoretical Physics, Universität Bonn, D-53115 Bonn, Germany

Abstract We amend a recent dispersive analysis of the anomalous η decay process $\eta \rightarrow \pi^+\pi^-\gamma$ by the effects of the a_2 tensor meson, the lowest-lying resonance that can contribute in the $\pi\eta$ system. While the net effects on the measured decay spectrum are small, they may be more pronounced for the analogous η' decay. There are nonnegligible consequences for the η transition form factor, which is an important quantity for the hadronic light-by-light scattering contribution to the muon's anomalous magnetic moment. We predict total and differential cross sections, as well as a marked forward-backward asymmetry, for the crossed process $\gamma\pi^- \rightarrow \pi^-\eta$ that could be measured in Primakoff reactions in the future.

Keywords Dispersion relations · Meson-meson interactions · Chiral Symmetries

PACS 11.55.Fv · 13.75.Lb · 11.30.Rd

1 Introduction

The decay $\eta \rightarrow \pi^+\pi^-\gamma$ is one of the processes driven by the chiral anomaly [1, 2]. The reduced scalar decay amplitude (to be defined below) in the SU(3) chiral limit and at vanishing momenta is given entirely in terms of the electromagnetic coupling e and the pion decay constant F_π ,

$$F_{\eta\pi\pi\gamma} = \frac{e}{4\sqrt{3}\pi^2 F_\pi^3} = 5.65 \text{ GeV}^{-3}. \quad (1)$$

Higher-order corrections to the anomaly can be evaluated in chiral perturbation theory [3], and pion-pion rescattering in the final state resummed effectively using dispersion theory [4]. Besides thus being an interesting decay in its own right to test our understanding of the interaction of light pseudoscalar mesons with

photons, this decay is particularly noteworthy as a fundamental ingredient in a dispersive analysis of the η transition form factor $\eta \rightarrow \gamma\gamma^*$ [5]. This quantity is a crucial input necessary for the ongoing program to analyze the hadronic light-by-light scattering contribution to the anomalous magnetic moment of the muon, combining as many pieces of experimental information as possible in a model-independent fashion [6, 7]. A similar analysis has also been pursued for the π^0 transition form factor [8].

As pointed out in Ref. [4], the decays of η and η' into $\pi^+\pi^-\gamma$ pose a beautiful and simple example to demonstrate the universality of final-state interactions. Neglecting (tiny) contributions of F and higher partial waves for the pion pair, the authors show that the reduced decay amplitude can be written as

$$\mathcal{F}(s, t, u) = P(t)F_\pi^V(t), \quad (2)$$

where $t = M_{\pi\pi}^2$ is the squared invariant mass of the pion pair, $F_\pi^V(t)$ denotes the pion vector form factor as measured in $e^+e^- \rightarrow \pi^+\pi^-$, and $P(t)$ is a polynomial. Comparison to experimental data obtained by the WASA-at-COSY [9] and KLOE [10] Collaborations demonstrated that within experimental accuracy, the polynomial can be assumed to be linear, $P(t) = A(1 + \alpha t)$, with [10]

$$\alpha = (1.32 \pm 0.13) \text{ GeV}^{-2}. \quad (3)$$

This result gives rise to several interesting questions. Obviously, Eq. (2) is only an approximation, tested successfully in the physical decay region, $4M_\pi^2 \leq t \leq M_\eta^2$. The universality of final-state interactions expressed therein is only valid in the region of *elastic* pion-pion rescattering, which is phenomenologically a good approximation up to roughly $t \approx 1 \text{ GeV}^2$. From generic considerations about the asymptotic behavior of the

decay amplitude, one would rather expect $P(t)$ to become constant for large t , such that the decay amplitude falls like $1/t$ similar to the asymptotic behavior of $F_\pi^V(t)$. The continuation beyond the physical regime is interesting in particular with regard to the application within a dispersive integral to obtain the η transition form factor [5], as in principle that integral covers all energies.

The present article is built on the following observation. If we continue the amplitude (2) naively to *negative* t , we ought to observe a zero at or near $t = -1/\alpha \approx -0.76 \text{ GeV}^2$. Such a kinematical regime is indeed accessible: in the crossed reaction $\gamma\pi^- \rightarrow \pi^-\eta$, which could be measured in a Primakoff-type reaction, i.e., the scattering of a charged pion in the strong Coulomb field of a heavy nucleus, producing an additional η . Such a Primakoff program is currently pursued by the COMPASS Collaboration (see, e.g., Ref. [11] for an overview), using a 190 GeV π^- beam and cutting on very small momentum transfers in order to isolate the photon-exchange mechanism from diffractive background. In this way, COMPASS can investigate $\gamma\pi^-$ reactions to various final states, in particular Compton scattering in order to extract the charged-pion polarizabilities [12, 13], $\pi^-\pi^0$ to investigate the chiral anomaly [14, 15], or three pions testing chiral predictions [16, 17]. In this paper, we want to provide the theoretical motivation to also measure the final state $\pi^-\eta$, as well as a prediction for the cross sections that are to be expected.

For this purpose, beyond using crossing symmetry, we need to amend the amplitude (2) for the following reason. The assumption underlying Eq. (2) is the neglect of so-called left-hand cuts: the two pions undergoing final-state interactions are assumed to originate from a point source, such that the amplitude is of form factor type, and any interaction (resonant or nonresonant) in the $\pi\eta$ channel is neglected. This approximation can be justified at low energies by appealing to chiral perturbation theory: the $\pi\eta$ P -wave is chirally suppressed (as well as all higher partial waves) [18, 19], an imaginary part only appears at three-loop order, any phase shift is therefore expected to be very small. Furthermore, the $\pi\eta$ P -wave has exotic quantum numbers $J^{PC} = 1^{-+}$, and the search for possible resonances in this channel is not fully conclusive so far [20, 21]. The first well-established resonance that is therefore going to be important in the process $\gamma\pi \rightarrow \pi\eta$ is the D -wave tensor meson $a_2(1320)$. To investigate its influence is important for several reasons:

- its inclusion will demonstrate to what extent the feature expected from Eq. (2), a zero (or at least a pronounced minimum) in certain differential cross

sections, can survive in a more complete description of the amplitude;

- it will provide a characteristic breakdown scale in the $\pi\eta$ invariant mass squared $s = M_{\pi\eta}^2$, above which $\pi\eta$ resonances dominate the cross section;
- finally, we can use the a_2 as the likely most important left-hand-cut structure for the decay $\eta \rightarrow \pi^+\pi^-\gamma$, to study to what extent it affects the decay amplitude, and whether its effect is consistent with the experimental decay data available.

The outline of this article is as follows. In Sect. 2, we recapitulate the dispersive representation of the $\eta \rightarrow \pi^+\pi^-\gamma$ decay amplitude of Ref. [4], before calculating contributions of the a_2 tensor meson first at tree level, then including pion–pion rescattering effects dispersively. Section 3 compares the resulting observables to the measured $\eta \rightarrow \pi^+\pi^-\gamma$ decay spectrum and briefly discusses the possible impact on the η transition form factor. In Sect. 4, we give our predictions for the crossed process $\gamma\pi^- \rightarrow \pi^-\eta$, discussing total and differential cross sections, the leading partial waves, as well as the resulting pronounced forward–backward asymmetry. We close with a summary. A brief discussion of the related decay $\eta' \rightarrow \pi^+\pi^-\gamma$ is relegated to an appendix.

2 $\eta \rightarrow \pi\pi\gamma$ with left-hand cuts

2.1 Amplitude, kinematics

We write the decay amplitude for the process

$$\eta(q) \rightarrow \pi^+(p_1)\pi^-(p_2)\gamma(k) \quad (4)$$

in terms of a scalar function $\mathcal{F}(s, t, u)$ according to

$$\mathcal{M}(s, t, u) = i\epsilon_{\mu\nu\alpha\beta}\epsilon^\mu(k)p_1^\nu p_2^\alpha q^\beta \mathcal{F}(s, t, u), \quad (5)$$

with the Mandelstam variables given as $s = (q - p_1)^2$, $t = (p_1 + p_2)^2$, and $u = (q - p_2)^2$. $\mathcal{F}(s, t, u)$ in the chiral limit fulfills the low-energy theorem $\mathcal{F}(0, 0, 0) = F_{\eta\pi\pi\gamma}$. The cosine of the t -channel center-of-mass angle is given by

$$\cos\theta_t = z_t = \frac{s - u}{\sigma_t(M_\eta^2 - t)}, \quad \sigma_x = \sqrt{1 - \frac{4M_\pi^2}{x}}. \quad (6)$$

The t -channel partial-wave expansion is of the form

$$\mathcal{F}(s, t, u) = \sum_{\text{odd } l} P'_l(z_t) f_l(t), \quad (7)$$

where $P'_l(z_t)$ denote the derivatives of the standard Legendre polynomials. Due to the strong suppression of F

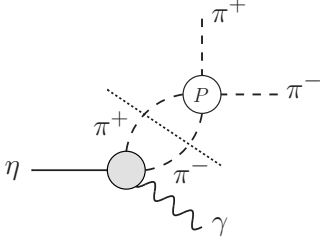


Fig. 1 Graphical illustration of the discontinuity equation (11). The gray circle denotes the t -channel P -wave projection of the $\eta \rightarrow \pi^+\pi^-\gamma$ decay amplitude, whereas the white circle stands for the P -wave pion-pion scattering amplitude.

and higher partial waves at low energies, we will almost exclusively be concerned with the P -wave, which is obtained by angular projection according to

$$f_1(t) = \frac{3}{4} \int_{-1}^1 dz_t (1 - z_t^2) \mathcal{F}(s, t, u). \quad (8)$$

The differential decay rate with respect to the pion-pion invariant mass squared is given by

$$\begin{aligned} \frac{d\Gamma}{dt} &= \Gamma_0(t) \times \frac{3}{4} \int_{-1}^1 dz_t (1 - z_t^2) |\mathcal{F}(s, t, u)|^2 \\ &= \Gamma_0(t) \times (|f_1(t)|^2 + \dots), \\ \Gamma_0(t) &= \frac{t\sigma_t^3(M_\eta^2 - t)^3}{12(8\pi M_\eta)^3}, \end{aligned} \quad (9)$$

where the ellipsis in the second line represents neglected higher partial waves.

In the absence of left-hand cuts and ignoring inelasticities, the P -wave should obey the following representation [4]:

$$f_1(t) = P(t)\Omega(t), \quad \Omega(t) = \exp \left\{ \frac{t}{\pi} \int_{4M_\pi^2}^{\infty} dx \frac{\delta(x)}{x(x-t)} \right\}, \quad (10)$$

where $\Omega(t)$ is the Omnès function [22] given in terms of the pion-pion P -wave phase shift $\delta(t) \equiv \delta_1^1(t)$, and $P(t)$ is a polynomial. The representation (10) is a solution to the discontinuity relation

$$\text{disc } f_1(t) = 2if_1(t) \sin \delta(t) e^{-i\delta(t)} \theta(t - 4M_\pi^2) \quad (11)$$

as obtained from elastic pion-pion rescattering; see Fig. 1. It obviously fulfills Watson's final-state interaction theorem [23]: the phase of $f_1(t)$ agrees with the elastic scattering phase $\delta(t)$. In the following, we will take $\delta(t)$ from the representation given in Ref. [24]. As already pointed out in the introduction, comparison with data [9, 10] suggested that the polynomial $P(t)$ is linear in the decay region,

$$P(t) = A(1 + \alpha_\Omega t), \quad (12)$$

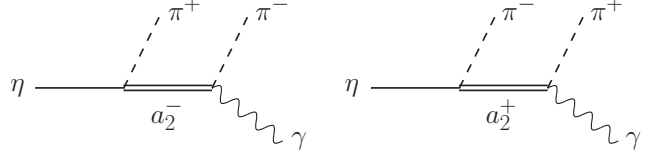


Fig. 2 Tree-level contributions of the $a_2(1320)$ resonance to $\eta \rightarrow \pi^+\pi^-\gamma$ in the s - (left) and u -channel (right).

to very good accuracy. In fact, in Ref. [4], the Omnès function was replaced by the pion vector form factor $F_\pi^V(t)$, which is a phenomenologically attractive representation insofar as the latter is itself directly experimentally observable. Both representations are equivalent modulo a moderate shift in the parameter $\alpha \rightarrow \alpha_\Omega$ due to the observation that the form factor is in turn proportional to the Omnès function up to a linear polynomial below 1 GeV, with a slope of the order of 0.1 GeV^{-2} [5].

2.2 Tree-level contribution of the $a_2(1320)$

We begin by calculating the tree-level contribution of the a_2 tensor meson to the amplitude $\eta \rightarrow \pi^+\pi^-\gamma$ as shown in Fig. 2. For the formalism of coupling tensor mesons to Goldstone bosons, we follow Ref. [25]. The single necessary interaction term required to describe the decay of a tensor meson into two pseudoscalars is given by

$$\mathcal{L}_{TPP} = g_T \langle T_{\mu\nu} \{u^\mu, u^\nu\} \rangle, \quad (13)$$

where $\langle \cdot \rangle$ denotes the trace in flavor space. For simplicity, we only display the nonstrange SU(2) part of the tensor field relevant to our calculation explicitly,

$$T_{\mu\nu} = \frac{1}{\sqrt{2}} \begin{pmatrix} a_2^0 & \sqrt{2}a_2^+ \\ \sqrt{2}a_2^- & -a_2^0 \end{pmatrix}_{\mu\nu} + \dots \quad (14)$$

The Goldstone bosons are encoded in the field $u_\mu = i(u^\dagger \partial_\mu u - u \partial_\mu u^\dagger)$ (neglecting external currents), where

$$u = \exp \left(\frac{i\phi}{2F_\pi} \right), \quad \phi = \begin{pmatrix} \pi^0 + \frac{\eta}{\sqrt{3}} & \sqrt{2}\pi^+ \\ \sqrt{2}\pi^- & -\pi^0 + \frac{\eta}{\sqrt{3}} \end{pmatrix} + \dots \quad (15)$$

From Eq. (13), we can calculate the decay width for $a_2 \rightarrow \pi\eta$, employing the polarization sum of the a_2 [25]

$$\begin{aligned} \sum_{\text{pol}} \epsilon_{\mu\nu}(l) \epsilon_{\rho\sigma}^*(l) &= P_{\mu\nu, \rho\sigma}(l), \\ P_{\mu\nu, \rho\sigma}(l) &= \frac{1}{2} (P_{\mu\rho} P_{\nu\sigma} + P_{\nu\rho} P_{\mu\sigma}) - \frac{1}{3} P_{\mu\nu} P_{\rho\sigma}, \\ P_{\mu\nu} &= g_{\mu\nu} - \frac{l_\mu l_\nu}{m_{a_2}^2}, \end{aligned} \quad (16)$$

and find

$$\Gamma(a_2 \rightarrow \pi\eta) = \frac{g_T^2}{180\pi F_\pi^4} \frac{\lambda^{5/2}(m_{a_2}^2, M_\pi^2, M_\eta^2)}{m_{a_2}^7}, \quad (17)$$

where $\lambda(a, b, c) = a^2 + b^2 + c^2 - 2(ab + ac + bc)$ denotes the usual Källén function. Equation (17), with the total width $\Gamma_{a_2} = (107 \pm 5) \text{ MeV}$ and the branching fraction $\mathcal{B}(a_2 \rightarrow \pi\eta) = (14.5 \pm 1.2)\%$ [26], leads to the coupling strength

$$|g_T| = (28.1 \pm 1.4) \text{ MeV}, \quad (18)$$

in perfect agreement with the number obtained in Ref. [25] from the decay $f_2 \rightarrow \pi\pi$ (compare also Ref. [27]), thus confirming SU(3) symmetry in this channel.

The coupling of the a_2 to pion and photon can be deduced from a Lagrangian (compare Refs. [28, 29])

$$\mathcal{L}_{TP\gamma} = -\frac{i c_T}{2} \epsilon_{\mu\nu\alpha\beta} \langle T^{\alpha\lambda} [f_+^{\mu\nu}, \partial^\beta u_\lambda] \rangle, \quad (19)$$

where $f_+^{\mu\nu} = u F^{\mu\nu} u^\dagger + u^\dagger F^{\mu\nu} u$ (omitting axial vector fields), $F^{\mu\nu} = eQ(\partial^\mu A^\nu - \partial^\nu A^\mu)$ is the electromagnetic field strength tensor, $Q = \text{diag}(2/3, -1/3, \dots)$ the quark charge matrix, and we have neglected additional currents. Equation (19) leads to the radiative decay width

$$\Gamma(a_2 \rightarrow \pi\gamma) = \frac{e^2 c_T^2}{160\pi F_\pi^2} \frac{(m_{a_2}^2 - M_\pi^2)^5}{m_{a_2}^5}, \quad (20)$$

which, compared to $\mathcal{B}(a_2 \rightarrow \pi\gamma) = (2.68 \pm 0.31) \times 10^{-3}$, leads to

$$|c_T| = (0.060 \pm 0.004) \text{ GeV}^{-1}. \quad (21)$$

If we combine the Lagrangians (13) and (19) with the tensor propagator $iP_{\mu\nu,\rho\sigma}(l)/(m_{a_2}^2 - l^2)$, we can calculate the a_2 -exchange contribution $\mathcal{F}_{a_2}(s, t, u)$ to $\eta \rightarrow \pi^+\pi^-\gamma$. We find

$$\begin{aligned} \mathcal{F}_{a_2}(s, t, u) &= \mathcal{G}(s, t, u) + \mathcal{G}(u, t, s), \\ \mathcal{G}(s, t, u) &= \frac{4ec_T g_T}{\sqrt{3}F_\pi^3} \frac{1}{m_{a_2}^2 - s} \\ &\times \left[t - u + M_\eta^2 - M_\pi^2 - \frac{(s + M_\pi^2)(M_\eta^2 - M_\pi^2)}{m_{a_2}^2} \right], \end{aligned} \quad (22)$$

which is completely fixed by experimental information up to an overall sign.

A few remarks are in order concerning Eq. (22). First, we can also perform an s -channel partial-wave expansion according to

$$\begin{aligned} \mathcal{F}(s, t, u) &= \sum_l P_l(z_s) g_l(s), \\ \cos \theta_s = z_s &= \frac{s(t - u) - M_\pi^2(M_\eta^2 - M_\pi^2)}{(s - M_\pi^2)\lambda^{1/2}(s, M_\eta^2, M_\pi^2)}, \end{aligned} \quad (23)$$

which is the natural partial-wave expansion for $\gamma\pi^- \rightarrow \pi^-\eta$ in terms of the scattering angle θ_s . The partial-wave expansion of the s -channel a_2 exchange amplitude $\mathcal{G}(s, t, u)$ then reads

$$\begin{aligned} \mathcal{G}(s, t, u) &= g_1^{a_2}(s) + 3z_s g_2^{a_2}(s), \\ g_1^{a_2}(s) &= \frac{4ec_T g_T}{\sqrt{3}F_\pi^3} \frac{(s + M_\pi^2)(M_\eta^2 - M_\pi^2)}{s m_{a_2}^2}, \\ 3z_s g_2^{a_2}(s) &= \frac{4ec_T g_T}{\sqrt{3}F_\pi^3} \frac{1}{m_{a_2}^2 - s} \left[t - u - \frac{M_\pi^2(M_\eta^2 - M_\pi^2)}{s} \right]. \end{aligned} \quad (24)$$

Phrased differently, $\mathcal{G}(s, t, u)$ contains a nonresonant P -wave contribution (which has no a_2 propagator) in addition to the expected resonant D -wave. This is a well-known problem of higher-spin propagators; see e.g. the discussion in Ref. [25]. We cannot easily subtract the P -wave and use the D -wave alone, as Eq. (24) shows that both partial waves individually display an artificial pole $\propto 1/s$, which is not present in the full amplitude (22). While a pole at $s = 0$ is not kinematically accessible in either of the two processes we consider in this article, it precludes a dispersive reconstruction of t -channel rescattering as discussed in the following section. We therefore retain the P -wave part in Eq. (24); its effect turns out to be numerically small.

Second, we fix the sign of $c_T g_T$ in the following way. As pointed out in Ref. [4], the vector-meson contributions to $\eta \rightarrow \pi^+\pi^-\gamma$ determined in Ref. [3] can be rewritten, using the limit of a large number of colors (i.e., neglecting loop effects) and expanding the ρ propagators to leading order in the spirit of resonance saturation of chiral low-energy constants, as

$$\begin{aligned} \mathcal{F}(s, t, u) &= F_{\eta\pi\pi\gamma} \left[1 + \frac{3t}{2m_\rho^2} + \mathcal{O}(m_\rho^{-4}) \right] \\ &= F_{\eta\pi\pi\gamma} \left[1 + \frac{t}{2m_\rho^2} \right] \Omega(t) + \mathcal{O}(m_\rho^{-4}), \end{aligned} \quad (25)$$

where we have used the approximation

$$\Omega(t) \approx \frac{m_\rho^2}{m_\rho^2 - t} = 1 + \frac{t}{m_\rho^2} + \mathcal{O}(m_\rho^{-4}). \quad (26)$$

In other words, Eq. (25) predicts $\alpha_\Omega^\rho \approx 1/(2m_\rho^2) = 0.84 \text{ GeV}^{-2}$, a little more than half of the phenomenological value $\alpha_\Omega \approx 1.52 \text{ GeV}^{-2}$ (when using Eq. (10) for the definition of α_Ω and not the pion vector form factor for α). We can now similarly expand Eq. (22) to leading order in inverse powers of $m_{a_2}^2$. If we neglect the induced quark mass renormalization of the anomaly (proportional to M_π^2, M_η^2), we find the following estimate for the a_2 contribution to α_Ω :

$$\alpha_\Omega^{a_2} = \frac{48\pi^2 c_T g_T}{m_{a_2}^2} = \pm(0.46 \pm 0.04) \text{ GeV}^{-2}. \quad (27)$$

We shall see below that the true effect when including the a_2 in a new extraction of the slope parameter α_Ω from data is significantly smaller, mainly due to curvature effects in the induced amplitude. Still, while effects in particular of excited ρ' resonances can be nonnegligible, we take the discrepancy between the ρ -induced slope and the experimentally determined value as an indication that the sign of the a_2 contribution ought to be positive,

$$c_T g_T = +|c_T g_T|. \quad (28)$$

The point of view of chiral perturbation theory allows us to further substantiate this choice. If we add the amplitude (22), expanded to leading order in $1/m_{a_2}^2$ and with the sign as in Eq. (28), as a further resonance saturation contribution to the one-loop representation of Ref. [3], the partial width $\Gamma(\eta \rightarrow \pi^+ \pi^- \gamma)$ increases by about 7 eV, bringing the original prediction of 47 eV into even better agreement with the experimental number (55 ± 2) eV [26]. We will therefore work on from this hypothesis, and we give further hints below that data indeed suggests this to be the more likely solution.

As a final remark, we will later insert a nonvanishing, energy-dependent width in the a_2 propagator in Eq. (22) by hand,

$$\frac{1}{m_{a_2}^2 - s} \longrightarrow \frac{1}{m_{a_2}^2 - s - i m_{a_2} \Gamma_{a_2}(s)}, \quad (29)$$

using the parametrization [30]

$$\begin{aligned} \Gamma_{a_2}(s) &= \Gamma_{a_2} \sum_{i=\eta, \rho} p_i \frac{m_{a_2}}{\sqrt{s}} \frac{q_i(s)}{q_i(m_{a_2}^2)} \frac{T(q_i(s)R)}{T(q(m_{a_2}^2)R)}, \\ q_{\eta/\rho}(s) &= \frac{\lambda^{1/2}(s, M_{\eta/\rho}^2, M_\pi^2)}{2\sqrt{s}}, \quad T(x) = \frac{x^4}{9 + 3x^2 + x^4}, \end{aligned} \quad (30)$$

which explicitly takes into account the a_2 decays into final states $\pi\eta$ and $\pi\rho$ with relative branching fractions $p_\eta = 0.17$, $p_\rho = 0.83$, using the barrier factor $R = 5.2 \text{ GeV}^{-1}$. The a_2 is sufficiently far from the $\pi\rho$ “threshold” that it seems a justifiable approximation to treat the ρ as a stable particle in this case. In contrast to using a constant width, this parametrization provides the correct threshold behavior of the imaginary part, as well as a reasonable phase above the resonance.

2.3 Unitarization

It is obvious that simply adding the tree-level a_2 contribution (22) to the original amplitude (10) violates Watson’s theorem: we are missing the pion–pion rescattering on top of the a_2 -exchange graphs; see Fig. 3. The

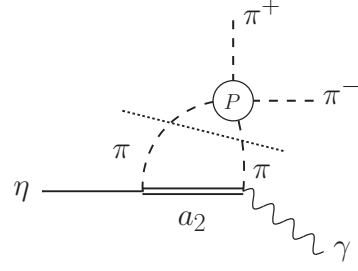


Fig. 3 a_2 contribution with pion–pion P -wave rescattering. The graph is supposed to comprise both possible charge assignments inside the loop, corresponding to tree-level s - and u -channel a_2 exchange; see Fig. 2.

full dispersive solution that reinstates the correct phase relation in the t -channel P -wave is of the form

$$\begin{aligned} \mathcal{F}(s, t, u) &= \mathcal{F}(t) + \mathcal{G}(s, t, u) + \mathcal{G}(u, t, s), \\ \mathcal{F}(t) &= \Omega(t) \left\{ A(1 + \alpha_\Omega t) \right. \\ &\quad \left. + \frac{t^2}{\pi} \int_{4M_\pi^2}^{\infty} \frac{dx}{x^2} \frac{\sin \delta(x) \hat{\mathcal{G}}(x)}{|\Omega(x)|(x-t)} \right\}, \\ \hat{\mathcal{G}}(t) &= \frac{3}{4} \int_{-1}^1 dz_t (1 - z_t^2) [\mathcal{G}(s, t, u) + \mathcal{G}(u, t, s)]. \end{aligned} \quad (31)$$

$\hat{\mathcal{G}}(t)$ is the projection of the a_2 exchange graphs onto the t -channel P -wave. It is given explicitly by

$$\begin{aligned} \hat{\mathcal{G}}(t) &= \frac{8ec_T g_T}{\sqrt{3}F_\pi^3} \left\{ \frac{M_\eta^2 - M_\pi^2}{m_{a_2}^2} - 1 + \frac{1}{M_\eta^2 - t} \left[m_{a_2}^2 \right. \right. \\ &\quad \left. \left. + 2t - 3M_\pi^2 - \frac{(m_{a_2}^2 + M_\pi^2)(M_\eta^2 - M_\pi^2)}{m_{a_2}^2} \right] Q(y) \right\}, \\ Q(y) &= \frac{3}{\sigma_t} \left(y + \frac{1 - y^2}{2} \log \frac{y + 1}{y - 1} \right), \\ y &= \frac{2m_{a_2}^2 - M_\eta^2 - 2M_\pi^2 + t}{\sigma_t(M_\eta^2 - t)}. \end{aligned} \quad (32)$$

$\hat{\mathcal{G}}(t)$ contains a square-root singularity at $t = 0$, signaling the onset of the left-hand cut. As $\hat{\mathcal{G}}(t)$ approaches a constant for large arguments $t \rightarrow \infty$, two subtractions in Eq. (31) are sufficient, as the Omnès function behaves asymptotically as $\Omega(t) \sim 1/t$ for $\delta(t) \rightarrow \pi$. The number of subtractions therefore exactly reflects the original form in Eqs. (10) and (12).

It is easy to see that the full t -channel P -wave resulting from Eq. (31),

$$f_1(t) = \mathcal{F}(t) + \hat{\mathcal{G}}(t), \quad (33)$$

has the correct phase, while $\mathcal{F}(t)$ alone is subject to the inhomogeneous discontinuity relation

$$\text{disc } \mathcal{F}(t) = 2i [\mathcal{F}(t) + \hat{\mathcal{G}}(t)] \sin \delta(t) e^{-i\delta(t)} \theta(t - 4M_\pi^2). \quad (34)$$

The representation (31), using the inhomogeneity $\hat{\mathcal{G}}(t)$ as input to the dispersive integral, preserves unitarity in the t -channel in the presence of left-hand cuts, which are approximated by resonance (here: a_2) contributions. This is closely related to the methods used e.g. in Ref. [29] for $\gamma\gamma \rightarrow \pi\pi$, or in Ref. [31] for semileptonic B -decays. We cannot easily apply an iterative procedure to determine left-hand cuts from right-hand cuts and vice versa, as done e.g. in the analysis of the closely related Primakoff process $\gamma\pi \rightarrow \pi\pi$ [15], as we do not have independent information on $\pi\eta$ scattering phases at our disposal.

Obviously, the a_2 s - and u -channel exchanges will also generate nonvanishing projections onto F - and higher t -channel partial waves. These partial waves are real as long as we neglect pion-pion rescattering effects in those higher waves, which is entirely justified for $\eta \rightarrow \pi^+\pi^-\gamma$ (and even for $\eta' \rightarrow \pi^+\pi^-\gamma$), given the smallness of the corresponding phases; compare the discussion in Ref. [32]. However, even the real part of the F -wave is entirely negligible: while in the chiral power counting, it is suppressed compared to the P -wave by another power of $p^2/m_{a_2}^2$, we have checked that kinematical prefactors effectively suppress it by more than 3 orders of magnitude in the physical decay region of $\eta \rightarrow \pi^+\pi^-\gamma$, and still by 2 for $\eta' \rightarrow \pi^+\pi^-\gamma$. We will therefore discuss the comparison to decay data in the following section still in the approximation indicated in Eq. (9), using the P -wave only.

3 Comparison to decay data

3.1 $\eta \rightarrow \pi^+\pi^-\gamma$ decay spectrum

In this section, we compare the amplitude constructed in the previous section to the data on $d\Gamma/dt$ as obtained by the KLOE Collaboration [10]. The decay distribution was measured with arbitrary normalization, which has to be fixed independently from the branching fraction $\mathcal{B}(\eta \rightarrow \pi^+\pi^-\gamma) = (4.22 \pm 0.08)\%$, as well as the total width of the η [26].

We first (re)fit the representation (10), (12). We obtain

$$\alpha_\Omega = (1.52 \pm 0.06) \text{ GeV}^{-2}, \quad (35)$$

where the error is only due to the statistical uncertainty in the data and neglects all the systematic effects discussed in Ref. [10]. The difference in the central value compared to α in Eq. (3) is due to employing the Omnès function instead of the pion vector form factor, as discussed above.¹ The quality of the fit is excellent,

¹In fact, if we construct the Omnès function from the phase of the pion vector form factor instead of from the $\pi\pi$ P -wave

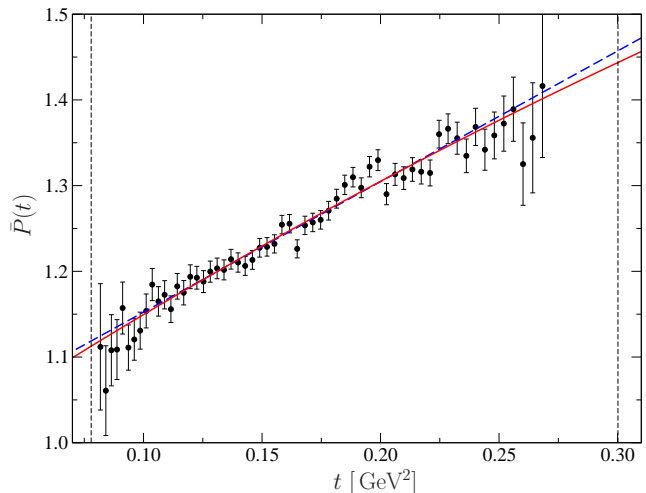


Fig. 4 Representation of the decay distribution $\eta \rightarrow \pi^+\pi^-\gamma$ from Ref. [10]; see main text for details. The blue dashed curve shows the linear fit, while the full red curve includes the effects of a_2 exchange in addition. The vertical dashed lines represent the limits of phase space at $4M_\pi^2$ and M_η^2 .

with a χ^2 per degree of freedom of $\chi^2/\text{ndof} = 0.94$. The subtraction constant A that, in this case, serves as an overall normalization of the amplitude, is $A = (5.43 \pm 0.12 \mp 0.04) \text{ GeV}^{-3}$, where the first error is due to the uncertainty in the integrated partial width, and the second due to the uncertainty in α_Ω , almost perfectly anticorrelated with the latter. A thus seems well compatible with $F_{\eta\pi\pi\gamma}$, see Eq. (1).

In Fig. 4, we plot the following observable, obtained from the data from Ref. [10]:

$$\bar{P}(t) = \sqrt{\frac{1}{\Gamma_0(t)} \frac{d\Gamma}{dt}} / [A\Omega(t)], \quad (36)$$

i.e. within the accuracy of the amplitude representation without left-hand cuts, we expect to find $\bar{P}(t) = P(t)/P(0) = 1 + \alpha_\Omega t$. As the quality of the fit suggests, the linear curve (blue dashed) describes the data perfectly.

Including the effects of a_2 exchange (properly unitarized in the t -channel), the subtraction constant α_Ω in Eq. (31) has to be refitted to the data. We obtain

$$\alpha_\Omega = (1.42 \pm 0.06) \text{ GeV}^{-2}, \quad (37)$$

with $\chi^2/\text{ndof} = 0.90$. The uncertainty of the a_2 coupling constants induces an additional error in α_Ω of $\pm 0.01 \text{ GeV}^{-2}$, which we will neglect in the following.

phase shift [24] as in Ref. [33], the central value of α_Ω reduces to 1.37 GeV^{-2} , rather close to Eq. (3). We disregard the effects of varying the $\pi\pi$ phase input in the following: they are compensated by corresponding shifts in α_Ω to a very large extent, and they lead to insignificant uncertainties compared to other error sources.

The resulting fit is also shown in Fig. 4. The reduction in the value of α_Ω compared to Eq. (35) may seem surprisingly small, given the estimate of the a_2 contribution to this parameter in Eq. (27). The reason is the curvature in $\bar{P}(t)$: in fact, the derivative $\bar{P}'(t)$ (which equals the constant α_Ω in the simple fit) varies from $\bar{P}'(4M_\pi^2) = 1.69 \text{ GeV}^{-2}$ to $\bar{P}'(M_\eta^2) = 1.30 \text{ GeV}^{-2}$ within the decay phase space; outside phase space, we find e.g. $\bar{P}'(1 \text{ GeV}^2) = 0.46 \text{ GeV}^{-2}$, and naive continuation to yet higher energies makes the derivative vanish and change sign around $\sqrt{t} = 1.25 \text{ GeV}$. It finally diverges at $t = 0$ due to the square-root singularity.

3.2 Impact on the η transition form factor

As far as the phenomenological description of the $\eta \rightarrow \pi^+\pi^-\gamma$ decay data of Ref. [10] is concerned, the two amplitudes, with and without a_2 effects included, are clearly equivalent: they describe the data equally well, and in fact, the two fit curves displayed in Fig. 4 deviate from each other by less than 1% in the whole decay region. This is different in the wider kinematic range of the similar decay $\eta' \rightarrow \pi^+\pi^-\gamma$, which we discuss in Appendix A. While the available data do not yet allow one to prefer one amplitude over the other in a statistically valid sense, the comparison of the extracted subtraction constants α_Ω and an α'_Ω defined in an analogous manner for $\eta' \rightarrow \pi^+\pi^-\gamma$ seems to favor somewhat the decay amplitude including the curvature effects induced by the a_2 .

However, we have emphasized in the introduction that the decay amplitude $\eta \rightarrow \pi^+\pi^-\gamma$ serves as a crucial input to a dispersive analysis of the η transition form factor [5], where the dispersion integral extends over a much larger range in energy (in principle, up to infinity). We therefore may expect to see a somewhat more significant deviation between the two amplitudes in there.

We refer e.g. to Ref. [5] for all pertinent definitions concerning the singly virtual η transition form factor $F_{\eta^*\gamma}(Q^2, 0)$, which at small photon virtualities can be expanded according to

$$\frac{F_{\eta^*\gamma}(Q^2, 0)}{F_{\eta^*\gamma}(0, 0)} = 1 + \left(b_\eta^{(I=1)} + b_\eta^{(I=0)}\right)Q^2 + \mathcal{O}(Q^4). \quad (38)$$

The slope parameter b_η is divided into an isovector $I = 1$ and an isoscalar $I = 0$ piece. The isoscalar part is small: employing $\omega + \phi$ dominance together with data input on $\omega, \phi \rightarrow \eta\gamma$ yields $b_\eta^{(I=0)} \approx -0.022 \text{ GeV}^{-2}$ [5]. The slope is therefore almost entirely given by the isovector contribution, which in turn is dominated by $\pi^+\pi^-$ intermediate states; see Fig. 5. The correspond-

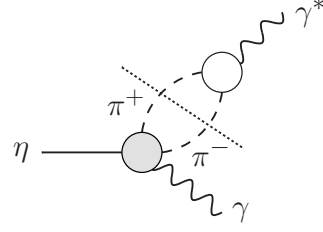


Fig. 5 Two-pion cut contribution to the isovector part of the (singly virtual) η transition form factor. Here, the gray circle denotes the t -channel $\eta \rightarrow \pi^+\pi^-\gamma$ P -wave, while the white circle is the pion vector form factor.

ing sum rule can be written as [5]

$$b_\eta^{(I=1)} = \frac{e}{96\pi^2 A_{\gamma\gamma}^\eta} \int_{4M_\pi^2}^{\Lambda^2} \frac{dx}{x} \sigma_x^3 F_\pi^{V*}(s) f_1(x), \quad (39)$$

where $F_\pi^V(t)$ is the standard pion vector form factor, and we have written the dispersion integral with a cut-off Λ^2 instead of integrating to infinity. The $\eta \rightarrow \gamma\gamma$ amplitude $A_{\gamma\gamma}^\eta$ is obtained from the corresponding partial width by

$$A_{\gamma\gamma}^\eta = \sqrt{\frac{64}{M_\eta^3}} \Gamma(\eta \rightarrow \gamma\gamma). \quad (40)$$

Following Ref. [5], we vary the cutoff in the range $\Lambda^2 = \{M_\eta^2, \dots, 2 \text{ GeV}^2\}$. With the decay amplitude (10), (12), we find

$$b_\eta^{(I=1)} = [2.04 \dots 2.22] \pm 0.04_\alpha \pm 0.02_B \pm 0.01_{F_\pi^V} \text{ GeV}^{-2}, \quad (41)$$

where the indicated range follows the range of cutoffs, and the errors are due to uncertainties in α_Ω ,² the branching ratios for $\eta \rightarrow \pi^+\pi^-\gamma$ and $\eta \rightarrow \gamma\gamma$, and the pion vector form factor. For the latter, we employ the pion vector form factor parametrizations of Refs. [33,34] (or approximations thereof). Using, however, the partial wave $f_1(t)$ as in Eq. (33), the result reduces to

$$b_\eta^{(I=1)} = [1.90 \dots 2.04] \pm 0.04_\alpha \pm 0.02_B \pm 0.01_{F_\pi^V} \pm 0.01_{a_2} \text{ GeV}^{-2}, \quad (42)$$

with the additional error due to the uncertainty in the a_2 coupling constants. That is, the slope is reduced by about 7%, a bit more than the combined error cited in Ref. [5], for a cutoff $\Lambda^2 \approx 1 \text{ GeV}^2$; this reduction is increased for higher cutoffs (due to the increasingly stronger curvature effects). A more detailed investigation of a_2 effects on the η (and η') transition form factor(s), beyond the value of the slope at the origin, should still be pursued.

²While we have propagated the statistical error on α_Ω from Eq. (35) only in the rest of this paper, we here use the larger uncertainty ± 0.13 due to systematic effects [10] in order to be consistent with the analysis in Ref. [5].

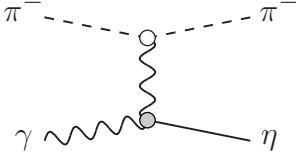


Fig. 6 Radiative correction to $\gamma\pi^- \rightarrow \pi^-\eta$ due to photon-exchange diagram.

4 Phenomenology for $\gamma\pi \rightarrow \pi\eta$

In the previous section, we have constructed an $\eta \rightarrow \pi^+\pi^-\gamma$ decay amplitude including the leading left-hand-cut contribution, and have shown that this amplitude describes the available decay data very well. As this representation includes the lightest resonance that can contribute in the $\pi\eta$ system, we are well equipped to now consider the crossed process

$$\gamma(k)\pi^-(p_2) \rightarrow \pi^-(\bar{p}_1)\eta(q), \quad (43)$$

which is described by the same amplitude as the decay process in Sect. 2 with $\bar{p}_1 = -p_1$ (using time-reversal invariance). The Mandelstam variables are defined as before, e.g. $s = (\bar{p}_1 + q)^2$ denotes the total energy squared in the center-of-mass system, $t = (p_2 - \bar{p}_1)^2$ is related to the pion momentum transfer etc. In particular, Eq. (23) is the natural partial-wave expansion in scattering kinematics.

The (polarization-averaged) differential cross section is given by

$$\frac{d\sigma}{d\Omega} = \frac{(s - M_\pi^2)\lambda^{3/2}(s, M_\pi^2, M_\eta^2)}{2048\pi^2 s^2} (1 - z_s^2) |\mathcal{F}(s, t, u)|^2, \quad (44)$$

from which one obtains for the total cross section

$$\begin{aligned} \sigma(s) &= \frac{(s - M_\pi^2)\lambda^{3/2}(s, M_\pi^2, M_\eta^2)}{1024\pi s^2} \\ &\times \int_{-1}^1 dz_s (1 - z_s^2) |\mathcal{F}(s, t, u)|^2 \\ &= \frac{(s - M_\pi^2)\lambda^{3/2}(s, M_\pi^2, M_\eta^2)}{768\pi s^2} \\ &\times \left[|g_1(s)|^2 + \frac{9}{5}|g_2(s)|^2 + \frac{18}{7}|g_3(s)|^2 + \dots \right], \end{aligned} \quad (45)$$

where we have inserted the s -channel partial-wave expansion (23) up to F -waves in the second step.

As a cautionary side remark, we wish to point out that it has been emphasized in Ref. [35] for the similar process $\gamma\pi^- \rightarrow \pi^-\pi^0$ that there is one significant effect due to radiative corrections, which is due to photon exchange in the t -channel, compare Fig. 6. Translated to

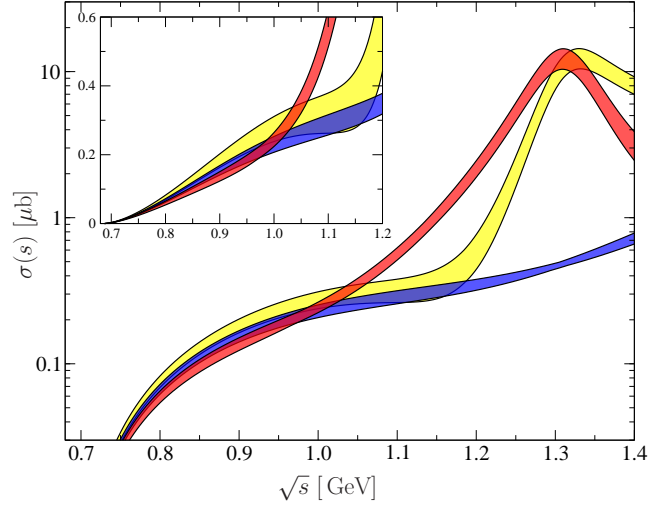


Fig. 7 Total cross section $\sigma(s)$ for $\gamma\pi^- \rightarrow \pi^-\eta$. The blue band shows the cross section obtained from crossing the decay amplitude of Ref. [4]; the red band corresponds to the full amplitude including a_2 effects. Finally, the yellow band displays the full cross section for the relative sign of the a_2 contribution flipped. The insert magnifies the near-threshold region. See main text on the error bands.

the process under investigation here, the inclusion of this effect amounts to correcting the scattering amplitude in the form

$$\mathcal{F}(s, t, u) \rightarrow \mathcal{F}(s, t, u) - \frac{2e}{t} A_{\gamma\gamma}^\eta. \quad (46)$$

Strictly speaking, the photon-exchange amplitude would have to be amended by form factor effects, including both the η transition and the pion vector form factor; however, these corrections were shown to be very small in $\gamma\pi^- \rightarrow \pi^-\pi^0$ [35]. The inclusion of the correction (46) may be desirable if experimental data on $\gamma\pi^- \rightarrow \pi^-\eta$ become sufficiently precise in the future; we still neglect it for the following investigation.

We show the total cross section in Fig. 7. We compare the cross section obtained from the decay amplitude in Ref. [4] by crossing to the full cross section including a_2 effects. We find that dominance of t -channel dynamics holds roughly up to $\sqrt{s} = 1$ GeV, while above this value, the tensor resonance begins to dominate. We predict a peak cross section of about $(12 \pm 2)\mu\text{b}$, which is of a similar order of magnitude as the cross section of $\gamma\pi^- \rightarrow \pi^-\pi^0$ at the ρ peak [15]. For completeness, we also display the cross section with the relative sign of the a_2 contribution, see Eq. (28), flipped (and all other parameters adjusted such as to best reproduce the $\eta \rightarrow \pi^+\pi^-\gamma$ decay data); we see that the transition from the near-threshold to the resonance region looks quite different, for reasons that will become transparent below. The uncertainty in the resonance peak is obviously dominated by those in the a_2 coupling constants

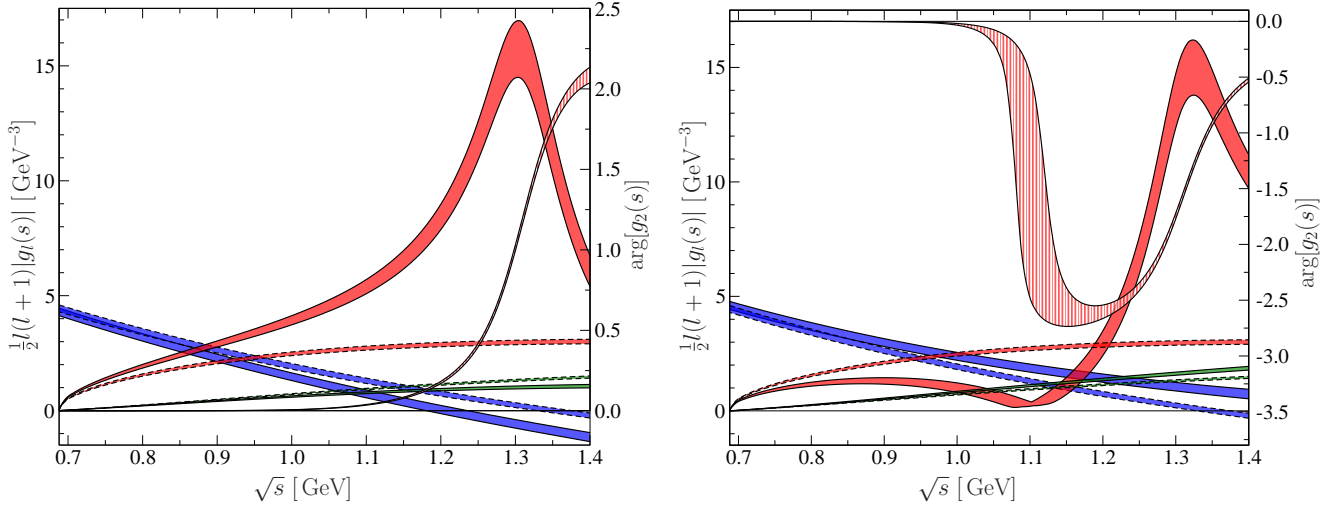


Fig. 8 First three partial waves for $\gamma\pi^- \rightarrow \pi^-\eta$. The moduli are shown in the normalization $\frac{1}{2}l(l+1)|g_l(s)|$ for P -wave (blue bands), D -wave (red), and F -wave (green); bands with dashed borders refer to the analytic continuation of the decay amplitude in Ref. [4], while the full bands show the full result including a_2 effects. The phase of the complete D -wave is represented by the red-striped band. All indicated bands combine the uncertainties in $\Gamma(\eta \rightarrow \pi^+\pi^-\gamma)$, α_Ω , and the a_2 couplings $c_T g_T$.

$c_T g_T$, while near threshold, the errors coming from the total decay rate $\Gamma(\eta \rightarrow \pi^+\pi^-\gamma)$ as well as α_Ω are more important.

In the introduction, we pointed out that a naive continuation of the $\eta \rightarrow \pi^+\pi^-\gamma$ decay amplitude Eqs. (10) and (12) would lead to a zero in the scattering amplitude $\gamma\pi^- \rightarrow \pi^-\eta$ at $t = -1/\alpha_\Omega$. As s increases, this zero first appears in the differential cross section $d\Gamma/dz_s$ in backward direction, i.e. for $z_s = -1$. Given the form of the partial-wave expansion (23),

$$\mathcal{F}(s, t, u) = g_1(s) + 3z_s g_2(s) + \dots, \quad (47)$$

and assuming F - and higher partial waves are small, this will occur once the D -wave is one third the size of the P -wave, as long as relative phases are small. In our amplitude representation, the only imaginary part stems from the energy-dependent width of s -channel a_2 exchange; the P -wave phase is neglected, and all partial waves induced by t -channel exchange are obviously real. For better comparison and due to

$$P'_l(-1) = \frac{(-1)^{l-1}}{2} l(l+1), \quad (48)$$

we display the first three partial waves multiplied with $\frac{1}{2}l(l+1)$ in Fig. 8; the intersection of P - and D -wave curves then gives an indication at the energy at which an additional zero in the angular distribution will occur, with the precise position slightly modified by the small, but nonnegligible F -wave. We compare the full amplitude including the a_2 to the continuation of the decay amplitude from Ref. [4]. The decisive observation is that including the a_2 , the D -wave becomes more important than the P -wave at even lower energies, around

$\sqrt{s} = 0.9$ GeV, where the phase is still tiny—we therefore indeed expect to observe an almost perfect vanishing of the amplitude. To demonstrate that this is not trivially so, Fig. 8 also shows what would happen with the opposite sign of the a_2 contribution: negative interference of s -channel a_2 and t -channel exchange leads to a near-vanishing of the D -wave around 1.1 GeV (which is the cause for the rapid phase variation at that energy), and its rise toward the a_2 peak only overtakes the P -wave once the phase is significant. As a consequence, no near-complete cancelation ever occurs at any energy.

We wish to re-emphasize that there is no fixed relation between the phase of our s -channel partial waves to $\pi\eta$ scattering phase shifts according to a final-state theorem. As the corresponding $\pi\eta$ phases are not theoretically determined in the way the $\pi\pi$ [24, 36, 37] or πK [38] phases are, unitarization using model phases seems to offer no significant improvement. Furthermore, the a_2 is a largely inelastic resonance with respect to $\pi\eta$ scattering anyway, with the dominant decay channel being $\pi\rho$ [see Eq. (30)], such that no simple version of Watson's theorem applies, and any unitarization would have to implement a coupled-channel formalism.

For illustration, we also show the resulting angular distribution at three sample energies $\sqrt{s} = 0.9$ GeV, 1.0 GeV, and 1.1 GeV in Fig. 9, indicating the transition between the threshold [P -wave dominance, $d\sigma/dz_s \propto (1 - z_s^2)$] and the resonance region [D -wave dominance, $d\sigma/dz_s \propto (1 - z_s^2)z_s^2$]. The very different features of the different signs of the a_2 are clearly visible.

An observable that allows one to capture the key features of the effect discussed even in a comparably low-statistics measurement is to characterize the be-

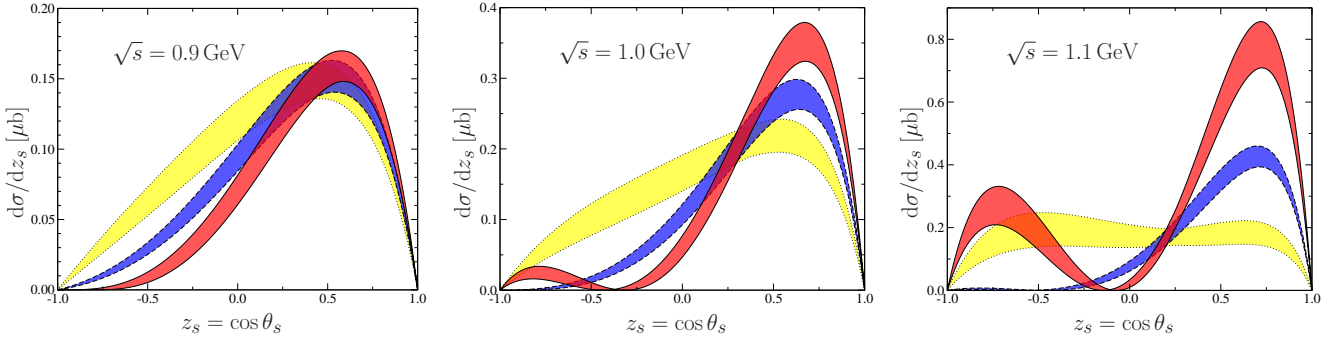


Fig. 9 Differential cross sections $d\sigma/dz_s$ for the three energies $\sqrt{s} = 0.9$ GeV, 1.0 GeV, and 1.1 GeV (from left to right). The blue bands denote analytic continuation of the amplitude of Ref. [4], the red bands are our full predictions including a_2 effects, while the yellow bands show the same with the opposite relative sign of the a_2 contributions. The pronounced minima, very close to actual zeros, in backward direction in the red bands are clearly seen.

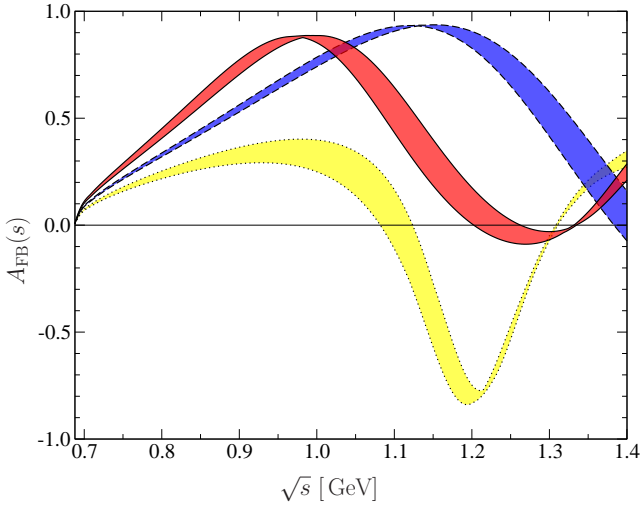


Fig. 10 Forward-backward asymmetry according to Eq. (49). The color code is as in Fig. 9.

havior in terms of a forward-backward asymmetry,

$$A_{\text{FB}}(s) = \sigma(s)^{-1} \left[\int_0^1 dz_s \frac{d\sigma}{dz_s} - \int_{-1}^0 dz_s \frac{d\sigma}{dz_s} \right] \simeq \frac{\text{Re}(g_2)(g_1 + g_3)}{\frac{4}{9}g_1^2 + \frac{4}{5}|g_2|^2 + \frac{8}{7}g_3^2}, \quad (49)$$

where in the second line we have neglected all partial waves beyond F -waves, as well as imaginary parts of the P - and the F -wave. As shown in Fig. 10, both the continuation of the decay amplitude without a_2 [4] and our full model with the preferred relative sign for the a_2 display a very large positive asymmetry, peaked just below $\sqrt{s} = 1$ GeV for the full model; for the opposite a_2 sign, the asymmetry is small near threshold, and subsequently even turns negative. An experimental verification of this asymmetry would therefore confirm that our description of the decay amplitude including the a_2 , and the resulting consequences for the η transition form factor, are indeed reasonable.

5 Summary

In this article, we have studied the effects of the a_2 tensor meson on the decay $\eta \rightarrow \pi^+\pi^-\gamma$ as well as the analytic continuation of the decay amplitude for the scattering process $\gamma\pi^- \rightarrow \pi^-\eta$. We have included the D -wave $\pi\eta$ resonance as a left-hand cut structure of a dispersive representation that obeys the correct final-state phase relation for the $\pi^+\pi^-$ P -wave. While the decay spectra measured by the KLOE Collaboration can be described equally well with and without the a_2 effects, there seems to be an indication for better consistency of the subtractions constants when comparing to the similar decay $\eta' \rightarrow \pi^+\pi^-\gamma$. The slope parameter of the resulting η transition form factor is reduced by about 7% in the dispersive integral up to 1 GeV² compared to a previous analysis [5].

We have predicted different observables for the η production reaction $\gamma\pi^- \rightarrow \pi^-\eta$ at energies up to the a_2 resonance. The peak cross section is predicted to be $(12 \pm 2)\mu\text{b}$, similar in size to the $\gamma\pi^- \rightarrow \pi^-\pi^0$ cross section in the ρ peak [15]. Fixing the relative sign of the a_2 to the more likely solution from decay phenomenology, we find an interesting P - D -wave interference effect, leading to almost perfect zeros in the differential cross section, and a very strong forward-backward asymmetry in the energy region between threshold and the a_2 peak. These predictions provide strong motivation to study the corresponding Primakoff reaction e.g. at COMPASS, which may help to further scrutinize the physics of light mesons relevant for hadronic corrections to the muon's anomalous magnetic moment.

Acknowledgements We would like to thank Christoph Hanhart, Martin Hoferichter, and Andreas Wirzba for useful discussions and comments on the manuscript, and Andrzej Kupść for supplying us with the acceptance-corrected data from Ref. [10]. Financial support by the DFG (SFB/TR 16, “Subnuclear Structure of Matter”) and the Bonn-Cologne

Graduate School of Physics and Astronomy is gratefully acknowledged.

Appendix A: $\eta' \rightarrow \pi\pi\gamma$

The formalism of dispersively analyzing decay data with a final-state P -wave pion pair was also applied to $\eta' \rightarrow \pi^+\pi^-\gamma$ in Ref. [4], analyzing data by the Crystal Barrel Collaboration [39]. We do not intend to make a prediction for the crossed Primakoff reaction $\gamma\pi \rightarrow \pi\eta'$ —the threshold is too high, too close to the a_2 resonance tail to still find traces of the t -channel exchange, and the number of inelastic (subthreshold) channels probably too large to be ignored. However, we expect the impact of left-hand cuts in the decay process to be much stronger over the wider kinematic range accessible in the η' decay, i.e., the curvature effects that are rather moderate in the η decay in Fig. 4 should be much more visible in that case. Furthermore, the decay $\eta' \rightarrow \pi^+\pi^-\gamma$ is about to be remeasured with increased precision by BESIII (see [40] for spectra not yet corrected for acceptance), such that a prediction for the curvature of the spectrum (after dividing out the universal Omnès factor) ought to be very timely.

To determine the a_2 contribution to $\eta' \rightarrow \pi^+\pi^-\gamma$, we first need to fix the $a_2 \rightarrow \pi\eta'$ coupling constant. We can first do this by naively defining a coupling g'_T without a Lagrangian, just through the analogous relation to Eq. (17)

$$\Gamma(a_2 \rightarrow \pi\eta') = \frac{(g'_T)^2}{180\pi F_\pi^4} \frac{\lambda^{5/2}(m_{a_2}^2, M_\pi^2, M_{\eta'}^2)}{m_{a_2}^7}, \quad (\text{A.1})$$

which, with $\mathcal{B}(a_2 \rightarrow \pi\eta') = (5.3 \pm 0.9) \times 10^{-3}$, yields

$$|g'_T| = (25.5 \pm 2.3) \text{ MeV}. \quad (\text{A.2})$$

If we attempt to explain this value based on the single Lagrangian term (13), we first need to amend the pseudoscalar field ϕ by the SU(3) singlet η_0 ,

$$\phi = \begin{pmatrix} \pi^0 + \frac{\eta_8 + \sqrt{2}\eta_0}{\sqrt{3}} & \sqrt{2}\pi^+ \\ \sqrt{2}\pi^- & -\pi^0 + \frac{\eta_8 + \sqrt{2}\eta_0}{\sqrt{3}} \end{pmatrix} + \dots \quad (\text{A.3})$$

In Eq. (15), we have simply identified the η with the octet field η_8 ; if now we assume a simple, single-angle $\eta\eta'$ mixing scheme,

$$\begin{aligned} |\eta\rangle &= \cos\theta|\eta_8\rangle - \sin\theta|\eta_0\rangle, \\ |\eta'\rangle &= \sin\theta|\eta_8\rangle + \cos\theta|\eta_0\rangle, \end{aligned} \quad (\text{A.4})$$

we can explain the ratio of the couplings by a mixing angle of $\theta = (-12.4 \pm 2.7)^\circ$, which is somewhat smaller than the standard value $\theta \approx -20^\circ$, but close enough

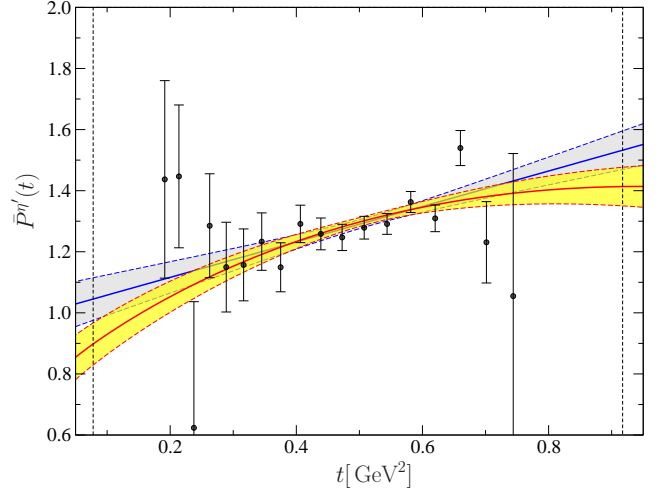


Fig. 11 Representation of the decay distribution $\eta' \rightarrow \pi^+\pi^-\gamma$ from Ref. [39]; see main text for details. The blue curve shows the linear fit, including the gray band for the fit uncertainty. The red curve with the yellow band includes the effects of a_2 exchange in addition. The vertical dashed lines represent the limits of phase space at $4M_\pi^2$ and $M_{\eta'}^2$.

that we are confident the difference can be explained by higher-order terms. In particular, we can safely conclude that the sign of g'_T in Eq. (A.2) agrees with the one of g_T .³

In Fig. 11, we display the observable $\bar{P}^{\eta'}(t)$ defined in strict analogy to Eq. (36), comparing the data of Ref. [39] to fits with a linear parametrization, as well as including effects of the a_2 . Due to the rather large error bars, we show the fit results as bands, not just the best fit. The linear fit leads to a slope parameter

$$\alpha'_\Omega = (0.6 \pm 0.2) \text{ GeV}^{-2}, \quad (\text{A.5})$$

with a reduced χ^2 of $\chi^2/\text{ndof} = 1.23$. It was argued in Ref. [4] that in the limit of a large number of colors, $\alpha_\Omega = \alpha'_\Omega$ should be expected, so the slopes of the polynomial would agree for η and η' decay. Comparing Eqs. (35) and (A.5), phenomenology seems rather at odds with this prediction. However, including the effects of the a_2 in the amplitude representation, we find much stronger curvature effects than for the η decay as anticipated, with the residual slope fitted to be

$$\alpha'_\Omega = (1.4 \pm 0.4) \text{ GeV}^{-2}, \quad (\text{A.6})$$

now with $\chi^2/\text{ndof} = 1.38$. The additional uncertainty due to the a_2 couplings is $\pm 0.1 \text{ GeV}^{-2}$. In this case, the fit quality becomes slightly worse (overall better

³As a side remark, we point out that fixing an effective $a_2 \rightarrow \pi\rho$ coupling constant from the known branching fraction $\mathcal{B}(a_2 \rightarrow \pi\rho)$ should also allow us to include a_2 effects in the decays $\eta' \rightarrow 4\pi$ [41, 42], thus going further beyond vector-meson dominance.

fits are essentially precluded by the third-to-last data point at $\sqrt{t} = [800, 825]$ MeV); however, α'_Ω is now in markedly better agreement with the value found for α_Ω in Eq. (37). $\bar{P}^{\eta'}(t)$ can be approximated in the decay region $4M_\pi^2 \leq t \leq M_\eta^2$ by a quadratic polynomial

$$\bar{P}^{\eta'}(t) \approx P^{\eta'}(0) \left(1 + \bar{\alpha}'_\Omega t + \bar{\beta}'_\Omega t^2 \right) \quad (\text{A.7})$$

to about 1% accuracy. The a_2 contribution predicts the curvature to be $\bar{\beta}'_\Omega = (-1.0 \pm 0.1) \text{ GeV}^{-4}$. As a side remark, we can also take this result as another strong indication on the correctness of the sign of $c_T g_T$ and $c_T g_T'$: a negative sign would lead to a residual slope α'_Ω of $(0.06 \pm 0.12) \text{ GeV}^{-2}$.

A more rigorous test of the decay spectrum predicted here, with higher-statistics data from BESIII, would be extremely welcome.

References

1. J. Wess and B. Zumino, Phys. Lett. B **37**, 95 (1971).
2. E. Witten, Nucl. Phys. B **223**, 422 (1983).
3. J. Bijnens, A. Bramon and F. Cornet, Phys. Lett. B **237**, 488 (1990).
4. F. Stollenwerk, C. Hanhart, A. Kupść, U.-G. Meißner and A. Wirzba, Phys. Lett. B **707**, 184 (2012) [arXiv:1108.2419 [nucl-th]].
5. C. Hanhart, A. Kupść, U.-G. Meißner, F. Stollenwerk and A. Wirzba, Eur. Phys. J. C **73**, 2668 (2013) [arXiv:1307.5654 [hep-ph]].
6. G. Colangelo, M. Hoferichter, M. Procura and P. Stoffer, JHEP **1409**, 091 (2014) [arXiv:1402.7081 [hep-ph]].
7. G. Colangelo, M. Hoferichter, B. Kubis, M. Procura and P. Stoffer, Phys. Lett. B **738**, 6 (2014) [arXiv:1408.2517 [hep-ph]].
8. M. Hoferichter, B. Kubis, S. Leupold, F. Niecknig and S. P. Schneider, Eur. Phys. J. C **74**, 3180 (2014) [arXiv:1410.4691 [hep-ph]].
9. P. Adlarson *et al.* [WASA-at-COSY Collaboration], Phys. Lett. B **707**, 243 (2012) [arXiv:1107.5277 [nucl-ex]].
10. D. Babusci *et al.* [KLOE Collaboration], Phys. Lett. B **718**, 910 (2013) [arXiv:1209.4611 [hep-ex]].
11. N. Kaiser and J. M. Friedrich, Eur. Phys. J. A **36**, 181 (2008) [arXiv:0803.0995 [nucl-th]].
12. J. Gasser, M. A. Ivanov and M. E. Sainio, Nucl. Phys. B **745**, 84 (2006) [hep-ph/0602234].
13. C. Adolph *et al.* [COMPASS Collaboration], Phys. Rev. Lett. **114**, 062002 (2015) [arXiv:1405.6377 [hep-ex]].
14. T. Nagel, Talk given at Hadron 2009, Tallahassee, Florida (2009). http://wwwcompass.cern.ch/compass/publications/talks/t2009/nagel_hadron09.pdf
15. M. Hoferichter, B. Kubis and D. Sakas, Phys. Rev. D **86**, 116009 (2012) [arXiv:1210.6793 [hep-ph]].
16. N. Kaiser, Nucl. Phys. A **848**, 198 (2010) [arXiv:1007.5277 [hep-ph]].
17. C. Adolph *et al.* [COMPASS Collaboration], Phys. Rev. Lett. **108**, 192001 (2012) [arXiv:1111.5954 [hep-ex]].
18. V. Bernard, N. Kaiser and U.-G. Meißner, Phys. Rev. D **44**, 3698 (1991).
19. B. Kubis and S. P. Schneider, Eur. Phys. J. C **62**, 511 (2009) [arXiv:0904.1320 [hep-ph]].
20. C. Adolph *et al.* [COMPASS Collaboration], Phys. Lett. B **740**, 303 (2015) [arXiv:1408.4286 [hep-ex]].
21. D. Schott [CLAS Collaboration], PoS **Confinement X**, 106 (2012).
22. R. Omnès, Nuovo Cim. **8**, 316 (1958).
23. K. M. Watson, Phys. Rev. **95**, 228 (1954).
24. R. García-Martín, R. Kamiński, J. R. Peláez, J. Ruiz de Elvira and F. J. Ynduráin, Phys. Rev. D **83**, 074004 (2011) [arXiv:1102.2183 [hep-ph]].
25. G. Ecker and C. Zauner, Eur. Phys. J. C **52**, 315 (2007) [arXiv:0705.0624 [hep-ph]].
26. K. A. Olive *et al.* [Particle Data Group Collaboration], Chin. Phys. C **38**, 090001 (2014).
27. M. Hoferichter, D. R. Phillips and C. Schat, Eur. Phys. J. C **71**, 1743 (2011) [arXiv:1106.4147 [hep-ph]].
28. F. Giacosa, T. Gutsche, V. E. Lyubovitskij and A. Faessler, Phys. Rev. D **72**, 114021 (2005) [hep-ph/0511171].
29. R. García-Martín and B. Moussallam, Eur. Phys. J. C **70**, 155 (2010) [arXiv:1006.5373 [hep-ph]].
30. G. M. Beladidze *et al.* [VES Collaboration], Phys. Lett. B **313**, 276 (1993).
31. X.-W. Kang, B. Kubis, C. Hanhart and U.-G. Meißner, Phys. Rev. D **89**, 053015 (2014) [arXiv:1312.1193 [hep-ph]].
32. F. Niecknig, B. Kubis, and S. P. Schneider, Eur. Phys. J. C **72**, 2014 (2012) [arXiv:1203.2501 [hep-ph]].
33. S. P. Schneider, B. Kubis and F. Niecknig, Phys. Rev. D **86**, 054013 (2012) [arXiv:1206.3098 [hep-ph]].
34. C. Hanhart, Phys. Lett. B **715**, 170 (2012) [arXiv:1203.6839 [hep-ph]].
35. L. Ametller, M. Knecht and P. Talavera, Phys. Rev. D **64**, 094009 (2001) [hep-ph/0107127].
36. B. Ananthanarayan, G. Colangelo, J. Gasser and H. Leutwyler, Phys. Rept. **353**, 207 (2001) [hep-ph/0005297].
37. I. Caprini, G. Colangelo and H. Leutwyler, Eur. Phys. J. C **72**, 1860 (2012) [arXiv:1111.7160 [hep-ph]].
38. P. Büttiker, S. Descotes-Genon and B. Moussallam, Eur. Phys. J. C **33**, 409 (2004) [hep-ph/0310283].
39. A. Abele *et al.* [Crystal Barrel Collaboration], Phys. Lett. B **402**, 195 (1997).
40. M. Ablikim *et al.* [BESIII Collaboration], Phys. Rev. D **87**, 092011 (2013) [arXiv:1303.7360 [hep-ex]].
41. F.-K. Guo, B. Kubis and A. Wirzba, Phys. Rev. D **85**, 014014 (2012) [arXiv:1111.5949 [hep-ph]].
42. M. Ablikim *et al.* [BESIII Collaboration], Phys. Rev. Lett. **112**, 251801 (2014) [Addendum-ibid. **113**, 039903 (2014)] [arXiv:1404.0096 [hep-ex]].